RSC Advances

ROYAL SOCIETY OF CHEMISTRY

www.rsc.org/advances

Journal Name

ARTICLE

Tuning the adsorption and separation properties of noble gases and N_2 in CuBTC by ligand functionalization

Received 00th January 20xx,
Accepted 00th January 20xx

DOI: 10.1039/x0xx00000x

www.rsc.org/

Zewei Liu,[a] Ying Wu,[a] Baoyu Liu,[a] Su Chen Oh,[b] Wei Fan,[c] Yu Qian[a] and Hongxia Xi[a*]

Grand Canonical Monte Carlo method was used to investigate the adsorption and separation properties of noble gas and N_2 mixtures on a MOF material, CuBTC, functionalized with different groups including amino, hydroxyl and fluorine in order to understand the potential applications of the materials in noble gas separation. Binary equimolar mixtures of Xe/Ar, Xe/Kr and Kr/Ar, as well as the nonequimolar mixtures of Xe/N_2 and Kr/N_2 containing 0.01% (molar fraction) noble gas were examined. Amino functionalized CuBTC displayed attractive interaction with all gases due to high polarity of amino-functionalized benzene and its large van der Waals interaction with all gases, while hydroxyl groups exhibit less impact on the adsorption properties of CuBTC. On the other hand, functionalization with fluorine groups largely decreased the adsorption capacity for all noble gases compared to the parent Cu-BTC. The functional groups also exhibited different effects on the adsorption selectivity to the noble gas over N_2. The amino functionalized CuBTC showed an enhanced selectivities towards noble gas over N_2 or other noble gases. Hydroxyl and fluorine groups exhibited similar selectivity with the original CuBTC. The difference in the adsorption selectivity is mainly attributed to the enhanced electron delocalization and the polarizability of the aromatic ring due to the presence of amino groups, which is the best binding sites for the noble gases and N_2. According to the simulation results, it can be concluded that amino groups functionalized CuBTC can enhance both the adsorption capacity and the selectivity of noble gas over N_2 or other noble gases at low pressure from 0 to 100kPa at 292K.

Introduction

Noble gases, which occupy only about 0.94% of the air with low chemistry reactivity, are now widely used in many fields such as tracer application[1], lighting[2], imaging[3], etc. For example, Ar, Kr and Xe are used to fill into light tube or windowpane due to their low thermal conductivity and high density. Xe is also applied as fuel in satellite launcher and narcotic in medical profession. However, noble gas only possesses fairly low concentration in the air, and their inertia chemical properties make them difficult to separate from the air or from each other. The current extraction methods for noble gases are cryogenic rectification, catalytic reaction and pressure swing adsorption (PSA). The former two methods are energetically expensive, while the low cost PSA is difficult to provide satisfying adsorption and separation performance due to the fully occupied valence shell of valence noble gases. Therefore, it is significant but also challenging to develop adsorption materials enable PSA to effectively purify and separate noble gas from the air.

Nanoporous adsorbents such as activated carbon[2], zeolites[4], molecular sieves[5] and single-walled carbon nanotube bundles[6, 7] are usually used for noble gas capture and purification. For example, Foroutan et al. studied adsorption behavior of ternary mixtures of noble gases inside single-walled carbon nanotube bundles, and found that heavier gases were more easily adsorbed than lighter ones on single-walled carbon nanotube bundles[6].

In the past few years, Metal-organic Frameworks (MOFs) have drawn extensive attention owing to their promising properties and tunable structures. Compared to other conventional nanoporous materials, MOFs have the advantage of high surface area, large pore volume, and tunable structure[8-10], which allow them to be deployed in many fields such as adsorption and separation[11] , catalysis[12] , ferromagnetic[13], florescence[14], drug carrier[15] , etc. One of the most significant applications of MOFs is gas adsorption and separation. So far there are few reports on adsorption and purification of noble gas by MOFs. Greathouse et al. reported adsorption and separation of noble gases in IRMOF-1 with Grand Canonical Monte Carlo (GCMC) simulation and found that selectivity of Xe to Ar or Kr may correlate with the van der Waals depth of each gas[16]. Thallapally compared adsorption of Xe on NIDOBDC and activated carbon, and they observed that NIDOBDC was more selective for Xenon over Krypton than activated carbon[2]. Parkes et al. studied the effect of pore size and framework topology on selective noble gas adsorption in air and discovered that heavier and more polarizable gases were more easily separated by MOFs than those lighter and less polarizable gases[17]. Wang et al.

[a] School of Chemistry and Chemical Engineering, South China University of Technology, Guangzhou 510640, PR China. Email: cehxxi@scut.edu.cn; Tel: +86 13825124468
[b] Department of Chemical and Biomolecular Engineering, University of Maryland, College Park, Maryland 20742, United States
[c] Department of Chemical Engineering, University of Massachusetts Amherst, 686 N. Pleasant Street, Amherst, MA 01002, USA.
†Electronic Supplementary Information (ESI) available. See DOI: 10.1039/x0xx00000x

compared adsorption and separation properties of Xe in several MOFs and COMs (Covalent-Organic Materials), concluding that Xe uptake on the materials is entirely consistent with their accessible surface area. In addition, the order of selectivities of Xe/N_2 on the materials follow the order of their difference in isosteric heats[18]. The recent studies imply that MOFs have potential benefits in adsorption and separation compared to the conventional adsorbents due to their tunable structures and compositions.

HKUST-1 (also called as CuBTC) was one of the well-studied MOFs, which was first reported by Chui et al. in 1999[19]. It consists of three types of cages including T1, L2 and L3cages (see Fig. 1). T1 cages (the small tetrahedral-shape pockets with diameter of 5-7Å) is surrounded by two large cages (L2 and L3 cages) that are formed by four BTC linkers and recognized as apolar in nature. L3 cages are larger (11-12Å) and more polar compared to L2 cages (10-13.5Å) due to the open copper site located inside the L3 cages. Its gas separation applications have been confirmed during the past decades[20-22]. Besides that, CuBTC can be easily synthesized using copper salt and terephthalate under mild condition[19]. Recent reports showed that CuBTC had high adsorption capacity for noble gas, exhibiting excellent potential for separating noble gases from the air or other noble gases[18, 23-25]. One unique feature of MOFs is the tunble functional groups on the surface, which can lead to a large variety of adsorption properties for gas adsorption. Therefore, functionalized MOFs have drawn significant attention for gas adsorption and separation over the past few years. For example, Couck et al. found that functionalized group can strengthen interaction between framework with CO_2, resulting in the enhanced affinity for CO_2[26]. Cai et al. investigated the impact of alkyl-functionalized BTC on adsorption and separation properties of copper-based CuBTC and

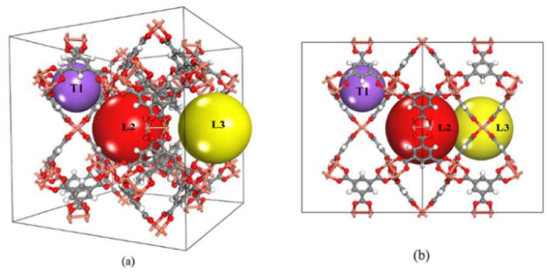

Fig. 1 The schematic of (a) 3-dimentional view and (b) left view of CuBTC model.

found that functionalized CuBTC was able to suppress water adsorption to one third of that in CuBTC while maintaining comparable CO_2 and CH_4 excess uptake up to 5 bar. It shows that proper functionalization on MOFs can promote the strong interaction between target gas with open-metal site in MOF and weaken that between water with open-metal MOF[27]. Obviously, functionalization is one of the effective methods that can be employed to tune MOFs with more promising properties on gas adsorption and separation. Due to the wide range of available ligands for MOFs systematical investigation of the relationship between structure and their adsorption and separation property using computational methods is highly desired. It is also more challenging to understand the impact of functionalization on MOFs for adsorbing noble gases because they are chemically inert substance without dipole moment and quadrupole.

Therefore, a GCMC simulation study was carried out to investigate the adsorption and separation properties of CuBTCs functionalized with different ligands. Three functionalized-CuBTCs were theoretical constructed by inserting fluorine, hydroxyl and amino groups onto aromatic ring of the organic linker. GCMC simulation were carried out to evaluate the adsorption and separation property of CuBTC and functionalized CuBTCs. The DFT calculation was employed to investigate the electrostatic potential of the cluster, preferred adsorption site and polarizability of the aromatic rings of the organic linker. The purpose of this work is to understand the noble gas adsorption on the fluorine, hydroxyl and amino functionalized CuBTCs and to investigate the potential applications of the materials in noble gas adsorption and separation.

Simulation details

Model construction and charge calculation

The crystal structure of CuBTC was constructed from the X-ray diffraction data. According to the previous report[28], the copper nodes and the ben-1,3,5-tricarboxylate (BTC) linkers construct the diametric copper paddle wheel, which is the structural building blocks for a three-dimensional face-centered CuBTC unit cell. Generally, the open-metal site is covered with hydroxyl group or other solvents which can be removed to form an activated framework.

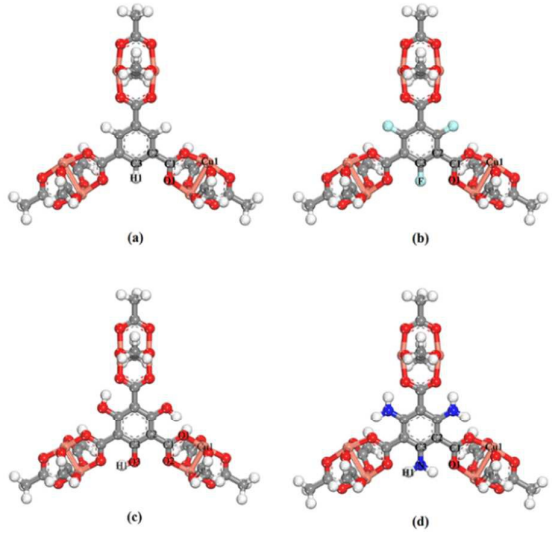

Fig. 2 The metal clusters for (a)CuBTC, (b)3F-CuBTC, (c)3OH-CuBTC and (d)$3NH_2$-CuBTC respectively. (copper: orange, oxygen: red, carbon: gray, hydrogen: white, nitrogen: dark blue, fluorine: light blue)

The X-functionalized (X=-F, -OH, $-NH_2$) CuBTC structures were constructed on the basis of its parent CuBTC. The original CuBTC metal cluster was cut down from CuBTC unit cell and methyl groups

was subsequently insert onto the nonsaturated site. The metal cluster of functionalized CuBTC was constructed by substituting the hydrogen atoms of the aromatic with the X groups. Finally the functionalized metal cluster was optimized by Gaussian 09[29] withwb97xd/6-311+g(2df,p) method (the same as those in binding energy calculation) for nonmetallic atoms and lan2ldz for copper and Xe atom while fixing the original structure and replicating the position of X groups onto CuBTC framework. This constructed model can be proper to accurately reflect X-functionalized CuBTC due to the unchanged symmetry after insertion of functionalized groups, which are small in size and have less impacts on the original CuBTC. The optimized metal clusters were displayed in Fig. 2. The similar styles of functionalization have been reported by other researchers. Katharina constructed an amino-functionalized CuBTC and discovered that it has the same tbo topology style with original CuBTC[30]. Yang et al. synthesised several functionalized CuBTC by functionalized origin one with groups including methyl, ethyl, methoxyl, bromo, nitro and acetamide and demonstrated that the last three functionalized CuBTC maintain the same topology structure with CuBTC[31]. The energy of the clusters and the energy gap (E_{gap}) between HOMO (Highest Occupied Molecular Orbital) and LUMO (Lowest Unoccupied Molecular Orbital) were listed in Table 1. The energy of the three functionalized clusters were slightly larger than that of original one, which may be contributed by the increasing atom numbers. However, the energy gap of the three functionalized clusters were smaller than that of original one, which demonstrated that the three functionalized clusters are more stable than the original one. Therefore, it is possible for the three functionalized CuBTC constructed in this article. Also, the same method was applied to calculate charges of atoms. The optimized clusters were fixed when charges were being calculated. All charges of atoms are given in the Table S1.

Table 1. Energy of four clusters and energy gap between HOMO and LUMO of four clusters.

Clusters	CuBTC	3F-CuBTC	3OH-CuBTC	3NH_2-CuBTC
Energy (a.u.)	-4030.78	-4327.4	-4255.2	-4080.1
E_{gap} (ev)	1.40	1.38	1.34	1.33

Force field

Potential parameters for MOFs were taken from mixed force field including the Universal Force Field (UFF)[32] and all-atom OPLS(OPLS-AA)[33] force field, which have been examined to be agreed with experiment results from Allendorf[34] . The model of noble gases referred to that used by Pellenq[35] and Levitz and Loef[36] . N_2 was defined as three-site model including two N atoms and a COM atom with van der Waals interactions and atomic charge reported by Siepmann[37] . All interatomic potential parameters were listed in Table S2. All the LJ cross interaction parameters were calculated by the Lorentz-Berthelot mixing rules:

$$\boldsymbol{\varepsilon_{ij}} = \left(\boldsymbol{\varepsilon_i \varepsilon_j}\right)^{1/2} \quad (1)$$

$$\boldsymbol{\sigma_{ij}} = \frac{1}{2}(\boldsymbol{\sigma_i} + \boldsymbol{\sigma_j}) \quad (2)$$

ε and σ represent energy well depth and van der Waals radii respectively.

GCMC simulation

Simulated adsorption isotherms were generated by the grand canonical Monte Carlo using the Music code from Snurr[38]. The lattice parameters of all MOFs are listed in Table S3, which was optimized by Forcite model of Materials Studio with ultrafine basis set[39]. The simulation was operated on 2×2×2 unit cells. Simulation was performed at 292K with pressure ranging from 1kPa to 100kPa. The excess uptake N_{ex} was transformed from the absolutely uptake N_{abs} to compare with experiment data by equation (reported Duren et al.[38]) as

$$\boldsymbol{N_{ex}} = \boldsymbol{N_{abs}} - \boldsymbol{\rho_g V_g} \quad (3)$$

Where $\boldsymbol{\rho_g}$ and $\boldsymbol{V_g}$ represent the density of the bulk gas calculated from PR EOS and the free pore volume of MOFs respectively. V_g was generated by the method of Myers et al.[40] from the ideal gas law:

$$\boldsymbol{V_g} = \frac{\boldsymbol{RN_mT}}{\boldsymbol{pm_m}} \quad (4)$$

Where R is the gas constant, T is the temperature, p is the pressure and N_m is the number of adsorbed probe molecules per molar mass m_m of the adsorbents, which is calculated by helium (σ=2.64 Å, ε/k_b=10.90K) gas in the MOFs at low temperature and ambient pressure.

The adsorption selectivity (S_{ads}) is often used to indicate the separation ability of nanoporous materials. The adsorption selectivity of component i over component j is defined as

$$\boldsymbol{S_{ads}} = \frac{\boldsymbol{x_i/x_j}}{\boldsymbol{y_i/y_j}} \quad (5)$$

where x and y represent the molar fraction of the two components in the adsorbed and bulk phase, respectively[41].

The binding energy (BE) was calculated to evaluate the interaction strength of gas molecules on different binding sites of adsorbents. In the optimizing process, the metal clusters were fixed in order to replicate bulk behavior while the gas molecules were near relaxed with the possible adsorption sites. The value of BEs can be given by the difference between the products and reactants including the energy of Basis Set Superposition Error (E_{BSSE})[42].

$$\mathbf{BE} = \boldsymbol{E_{MOF-gas}} - \boldsymbol{E_{MOF}} - \boldsymbol{E_{gas}} + \boldsymbol{E_{BSSE}} \quad (6)$$

where $\boldsymbol{E_{MOF-gas}}$ is the total energy of the adsorbate –adsorbent system in equilibrium state, while $\boldsymbol{E_{MOF}}$ and $\boldsymbol{E_{gas}}$ are the non-adsorbed MOF structure and gas molecule, respectively.

Results and discussion

Adsorption isotherms

Single component adsorption isotherms of different gas molecules on CuBTC at 292K were first simulated, and compared to experimental data (Fig. 3). The experiment data was obtained from the work of Allendorf et al[34]. Although a slight difference exists between simulations and experiment data, the GCMC simulation can still reproduce the experiment results with certain accuracy, indicating that the force field used in this study is reasonable for simulating adsorption and separation properties of CuBTC and the functionalized CuBTCs. Previous work has also confirmed that such results can match well with experiment data[34]. Overall the force field is reasonable for simulating adsorption and separation properties of CuBTC and the functionalized CuBTCs.

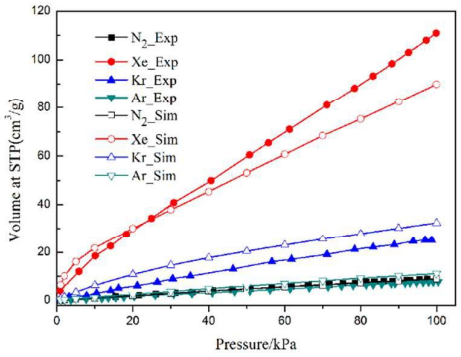

Fig. 3 Comparison of experimental and simulation N_2 and noble gases adsorption isotherms at 292K.

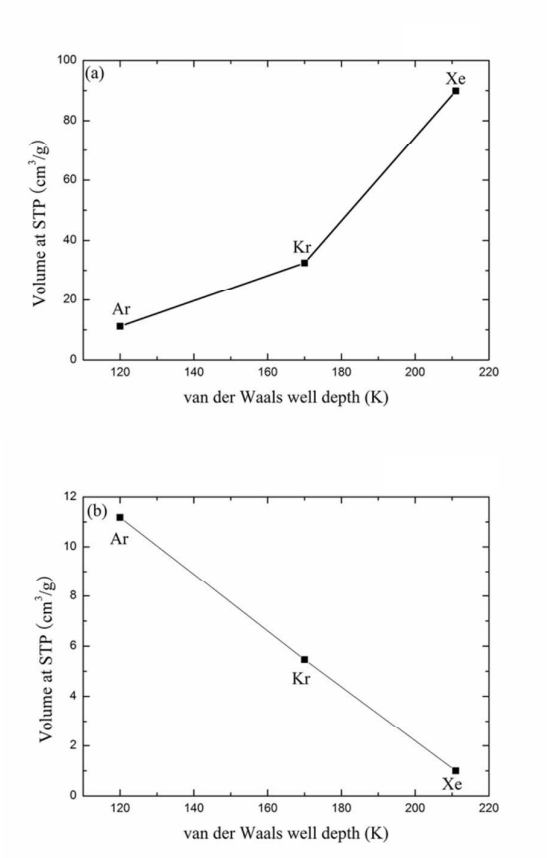

Fig. 4 Comparison of the adsorption and separation property of noble gases by ε. (a) Comparison between ε and adsorption volume of noble gas at 100kPa; (b) Comparison between ε and selectivities of Xe over Kr and Ar at 100kPa.

Since the outer shell of noble gas atoms is full occupied by electrons and the atoms are spherically symmetric, coulomb interactions, dipole–dipole interactions and hydrogen-bonding interactions have little effects on the binding between noble gases and the MOFs. The charge induced, dipole-induced and dispersion forces may, however, play roles on the adsorption of noble gases. Both experiment and simulation results suggest that the adsorption of noble gases on CuBTC favors for molecules. This result may be due to the different electronic polarizability, the size and the van der Waals well depths (ε) of the noble gas atoms. The electronic polarizability of Xe, Kr and Ar, which were expressed in units of $(4\pi\varepsilon)$ Å, were reported as 4.04, 2.48 and 1.63 respectively[43]. The electronic polarizability can result in the displacement of the electron cloud. The larger the displacement is, the more inducible interaction will happen in the adsorption process. Therefore, Ar and Kr showed lower interaction with known binding sites in the CuBTC compared to Xe. In addition, the ε of the noble gas atoms may affect their adsorption properties in the framework. Greathouse compare to the van der Waals well depths of Xe, Kr and Ar with the experimental data, and found out that noble gas with larger van der Waals well depth tends to be preferentially adsorbed by adsorbents at low pressure[16]. Fig. 4 compares the adsorption capacity of CuBTC for Ar, Kr and the adsorption selectivity to Xe in equimolar Xe/Kr and Xe/Ar mixtures at 100kPa using the van der Waals well depths as a coordinator. The results clearly suggest that the adsorption capacity is correlated to the van der Waals well depth. A similar correlation was also observed for the van der Waals diameter σ (listed in Table S2). Therefore, we conclude that the adsorption capacity for noble gas on the CuBTC closely correlates with the ε and σ of the noble gas atoms. Xe selectivity is larger in the Xe/Ar mixture due to the ratio of $\varepsilon_{Xe}/\varepsilon_{Ar}$ is larger than $\varepsilon_{Xe}/\varepsilon_{Kr}$. Since N_2 (the main composition of the air) is nonpolar gas with a little quadrupole, N_2 can be treated as an inert gas to a certain degree.

Table 2 The structural parameters of CuBTCs

MOF	Pore volume(cm^3/g)	$S_{acc}(m^2/g)$	$\rho_{crystal}(g/cm^3)$
CuBTC	0.879	1924.49	0.805
3F-CuBTC	0.708	1774.92	1.010
3OH-CuBTC	0.711	1787.92	1.014
$3NH_2$-CuBTC	0.683	1701.00	1.034

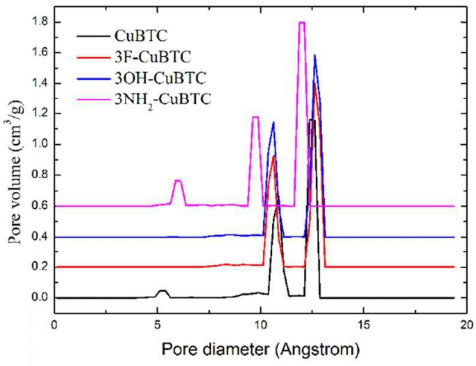

Fig. 5 The comparison of pore diameter distribution of CuBTCs.

When the functionalized groups were introduced into the original CuBTC metal cluster, it was observed that the angle between that C-X bond (X groups with aromatic carbon atoms) and

aromatic plane is consistent with that between the C-H bond with aromatic plane in the original CuBTC metal cluster. The structural properties of X-CuBTC and CuBTC including the accessible surface area (S_{acc}), pore volume (V_p), and density of MOFs (ρ_{MOF}) were displayed in Table 2. The pore size distribution(PSD), listed in Fig. 5, was calculated from Poreblazer code developed by Sarkisov et al[44]. The S_{acc} and V_p are decreased with the addition of functional groups into the framework. Noticeably, larger functional group (-NH_2>-OH=F) led to smaller S_{acc} and V_p. As shown in the pore size distributions (Fig. 5), the peaks are assigned as T1, L2 and L3 cage type from left to right respectively. The T1 cages centered at 5 Å are invisible in the 3OH-CuBTC and 3F-CuBTC, indicating that the small cages can be easily blocked by the functional groups. This implies that the presence of inserted groups gives rise to the steric hindrance effect in the small T1 cages. In contrast, the –OH and -F groups didn't effect on the size distribution of L2 cages(the peak centered at 11 Å) and L3 cages(the peak centered at 11 Å), suggesting that there are no functional groups in the L2 cages and L3 cages of these two functionalized CuBTCs. Interestingly, the diameter of T1 cages in $3NH_2$-CuBTC increased to 5.9 Å while the diameter of L2 and L3 cages decreased to 9.7 Å and 12 Å respectively. The enlargement of the T1 cages may be attributed to the gas adsorption of MOF at low pressure and the reduction of L2 and L3 cages in size may increase the interaction between gas and MOF. Commonly, when the gas is adsorbed in the L2 and L3 cages the MOF may prefer to adsorb the larger gas due to its larger dynamic diameter. The gas would diffuse into the L2 and L3 cages after the T1 cages were filled. Therefore, the reduction of L2 and L3 cages in the $3NH_2$-CuBTC would do help to the larger gas at high pressure. In addition, the functionalize groups can induce steric hindrance effect in the adsorption of noble gases and N_2.

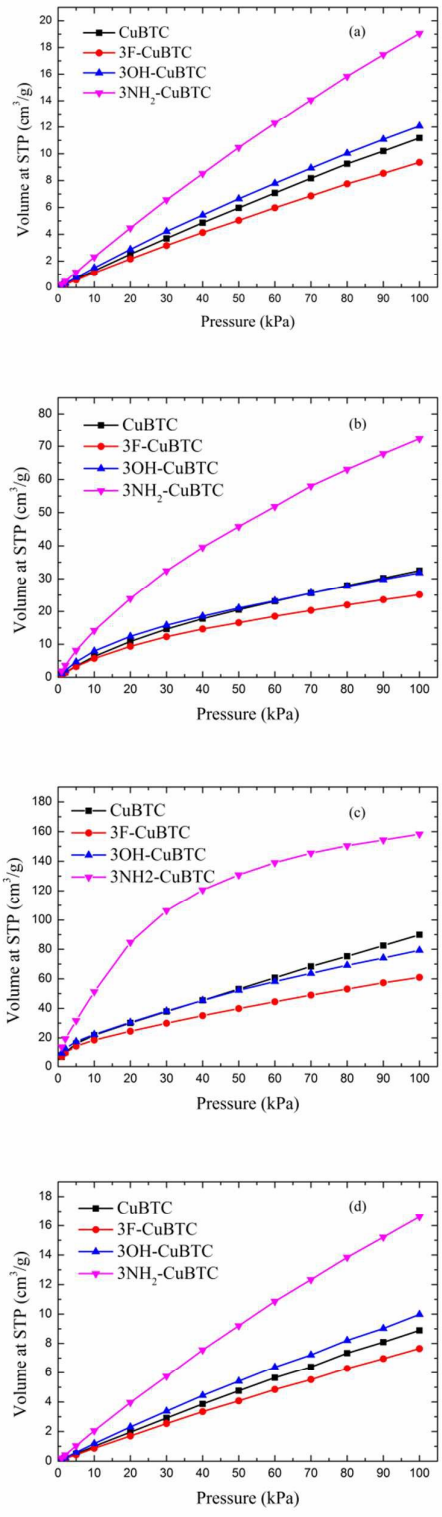

Fig. 6 Adsorption isotherms of (a)Ar, (b)Kr, (c)Xe and (d)N_2 at 292K.

Fig. 6 depicted the adsorption isotherms of noble gases and N_2 on CuBTCs with different functional groups from 0 to 100kPa at 292K. Among the three CuBTC samples, $3NH_2$-CuBTC exhibited the highest adsorption capacities for all studied gases. 3OH-CuBTC showed similar adsorption properties with the parent CuBTC, while 3F-CuBTC exhibited relatively weak adsorption for the gases. The order of the polarity of the functionalized groups is F>OH>NH_2. The low adsorption capacity of 3F-CuBTC for noble gas is constructive since the noble gas atoms or the N_2 atoms would be favorably adsorbed on the atom or groups with higher polarizability. This may suggest that noble gases and N_2 were not preferred to be adsorbed near the functional groups, in particular at low pressure. In order to understand the adsorption properties of the functionalized CuBTC, the polarizabilities of functionalized aromatic ring were calculated (listed in Table 3). The increased polarizability follows the order of benzene, 3F-benzene, 3OH-benzene and $3NH_2$-benzene, which is in agreement with the order of the enhanced value of adsorption volume of noble gases and N_2 at low pressure except for the 3F-benzene. This indicates that the noble gases and N_2 are

Table 3. Polarizability of the functionalized benzenes derivatives

Benzenes	Polarizability($C \cdot m^2/V$)
Benzene	70.55
3F-benzene	70.82
3OH-benzene	88.12
$3NH_2$-benzene	103.49

preferentially adsorbed on the aromatic planes of the CuBTC with different functional groups. The lower capacity for 3F-CuBTC can be attributed to the similar polarizability between benzene and 3F-benzene but the much higher weight of fluorine atom compared to hydrogen atom. We also observed that the adsorption capacity of gases is correlated with the van der Waals well depth of the center atoms of functionalized groups. Fig. 7 compared the adsorption volume of gases at 100 kPa in CuBTCs by using the ε of the center atoms of functionalized groups and hydrogen atom. There is a remarkable relationship between the van der Waals of noble gas with its adsorption volume at 100kPa. In other words, the inserted group with larger van der Waals depth contributed more to the adsorption volume of each gas. Although the van der Waals well depth of F atom is larger than that of hydrogen atom, the adsorption volume of each noble gas on CuBTC is larger than that on 3F-CuBTC. It was likely associated with the 16 times larger molecular weight of F atom than that of hydrogen atom, which made larger effect than the van der Waals well depth on the adsorption property.

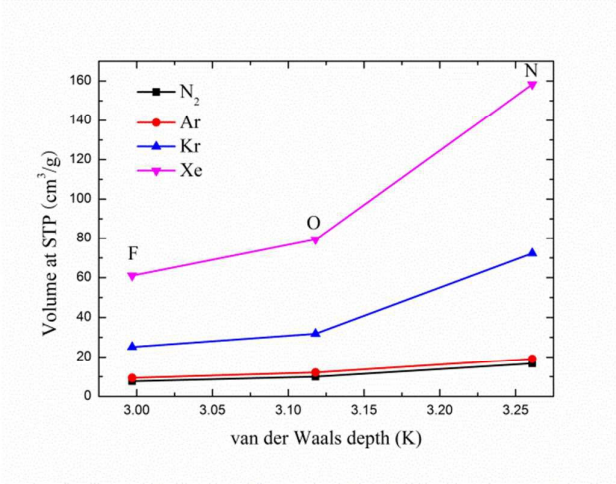

Fig. 7 Comparison of adsorption volume of noble gases and N_2 at 100kPa by the van der Waals depth of center atom of the functionalized groups.

Preferential adsorption sites

As shown in Fig. 8, snapshots from production simulation were undertaken to further understand the adsorption mechanism of noble gases and N_2 on the adsorbents with different functionalized groups. Fig. 8(e)-8(h) indicates that each gas was preferentially adsorbed in the T1 cages of CuBTC, which subsequently diffuse into L3 cages after T1 cages were mostly filled. Some of them were adsorbed in L2 cages due to the polarizability regions surrounding the open copper atoms. As we can see, most of gases were preferentially adsorbed above the center of the organic linker in CuBTC. Similar phenomenon was found in $3NH_2$-CuBTC. As shown in Fig. 8(a)-8(d), the insertion of amino groups enhanced the adsorption amount of Xe in $3NH_2$-CuBTC. This phenomenon was attributed by the enhancement in polarizability of the linker and the reduction in size of L2 and L3 cages. At low pressure, the enhancement in polarizability polarized adsorbed gases, which enhance the interaction between gas atoms with linkers and accelerate the filling of T1 cages. Also, the reduction in size of L2 and L3 cages could decelerate the diffusion of Xe in $3NH_2$-CuBTC and enhance the interaction between gas atoms with the framework. In addition, noble gases mainly centered in T1 pockets and L3 pockets, which indicated that noble gases were preferentially bound with aromatic rings or the carbon site that connected with the aromatic ring. Similar phenomenon was found on the other functionalized groups.

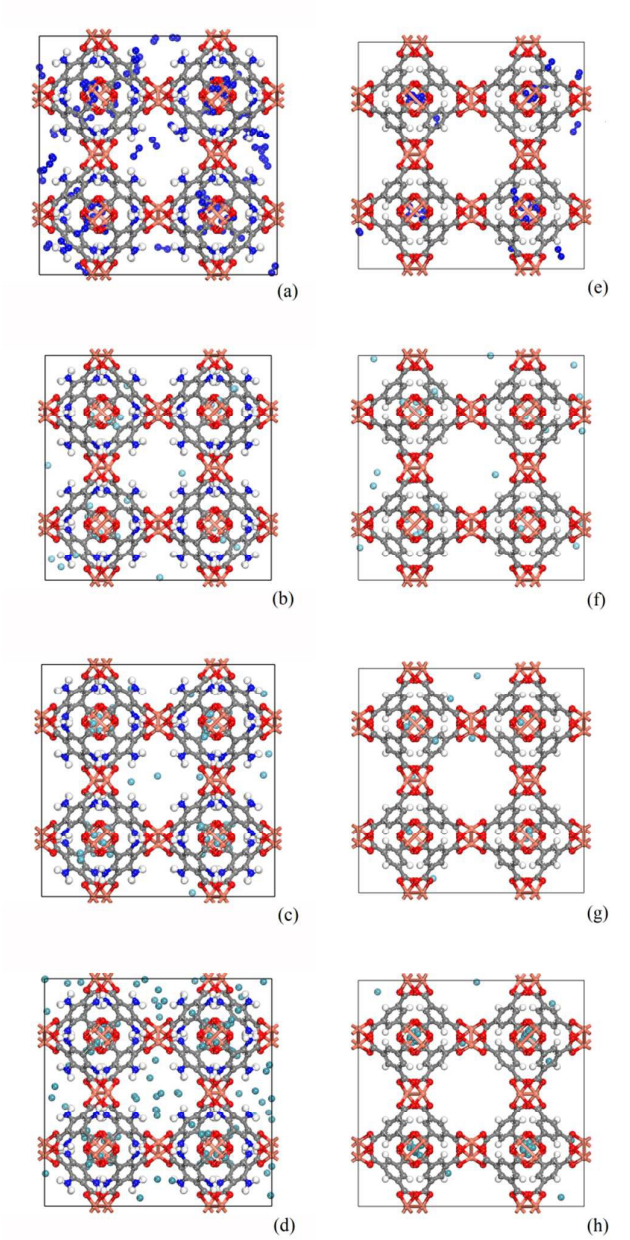

Fig.8 Comparison of snapshots of $3NH_2$-CuBTC and CuBTC.(a)-(d) represent N_2 at 100kPa, Ar at 50kPa, Kr at 10kPa and Xe at 5kPa in $3NH_2$-CuBTC respectively,(e)-(g) represent N_2 at 100kPa, Ar at 50kPa, Kr at 10kPa and Xe at 5kPa in CuBTC respectively. (copper: orange, oxygen: red, carbon: gray, hydrogen: white, nitrogen: dark blue, fluorine: light blue, noble gas: light blue, N_2: dark blue)

We predicted the possible binding site by comparing the binding energy in different binding sites. There may be two binding sites (in

Fig. 9) in the process of adsorbing noble gases. One is the aromatic ring site (L-site) and the other one is the C-site. After the optimization of adsorption distance, it was found that the noble gas atoms preferred to stay above the aromatic rings and moved away from the C-site. Here we calculated the biding energy of Xe with the L-site of $3NH_2$-CuBTC and CuBTC clusters. The data showed that $E_{3NH2\text{-}CuBTC}$ was -8.319 kJ/mol while E_{CuBTC} was -0.035kJ/mol. The insertion of amino groups greatly increased the binding energy of Xe with the clusters, which indicates that the amino group can significantly enhance the interaction of gas atoms with the aromatic rings (L-site).

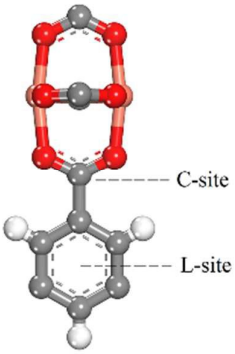

Fig. 9 The possible binding site of noble gases and N_2 in CuBTC at low pressure.

Adsorptive selectivities

Ideal adsorbed solution theory (IAST) of Myers and Prausnitz[45] was applied to calculate the adsorption selectivities of noble gase over N_2 or other noble gas. IAST, which assumes that the adsorbed mixture is an ideal solution with constant temperature and pressure, has been widely used to predict the adsorption selectivities of binary gas mixtures from pure component isotherms[46-48]. According to IAST, the chemical potential of the adsorbed solution is considered to be equal to that of the gas phase at equilibrium[45].

Fig. 10 and Fig. 11 display adsorption selectivities of various noble gases and N_2 on the four types of CuBTCs. For the three types of selectivities in Fig.10, there was a visible enhancement on $3NH_2$-CuBTC when the pressure is lower than 20 kPa, while selectivity didn't change significantly with increasing pressure. The similar phenomenon was observed on the other three functionalized CuBTCs. The diameter of L2 and L3 cages of 3OH-CuBTC is equal to that of 3F-CuBTC, but the polarizability of 3OH-benzene is larger than that of 3F-CuBTC. The larger polarizability would enhance the interaction between the larger gas atoms with the benzene of L2 and L3 cages at high pressure. Therefore, it can be found that all the selectivities of 3OH-CuBTC were larger than that of 3F-CuBTC. Fig. 11 shows the selectivity for CuBTCs for Xe/N_2 and Kr/N_2 mixture including 99% molar fraction for N_2. For the adsorption selectivity of Xe on N_2, $3NH_2$-CuBTC showed outstanding performance compared with the other three CuBTCs. Since the molar fraction of N_2 is high, a slight change in the adsorption amount of Xe might help in enhancing the selectivity of Xe/N_2. The adsorption volume of Xe in $3NH_2$-CuBTC is nearly twice that in CuBTC. Therefore, $3NH_2$-CuBTC is the best adsorbents among these three functionalized CuBTCs. The selectivity of Xe/Ar, Xe/Kr, K/Ar and each noble gas over N_2 decreased with the increasing pressure, which can be attributed to the difference of the molecular dynamic diameter of each gas(N_2:3.64Å, Ar:3.542 Å, Kr:3.655 Å, Xe:4.047 Å). With the increasing pressure, the smaller gas atoms have an advantage to flow into the L2 cage or L3 cage than the larger gas atoms, resulting in the decrease in selectivity. In addition, for the selectivity of noble gas over N2, there was little interaction between N_2 atoms. Therefore the competitive adsorption ability of the larger molecules would be minified.

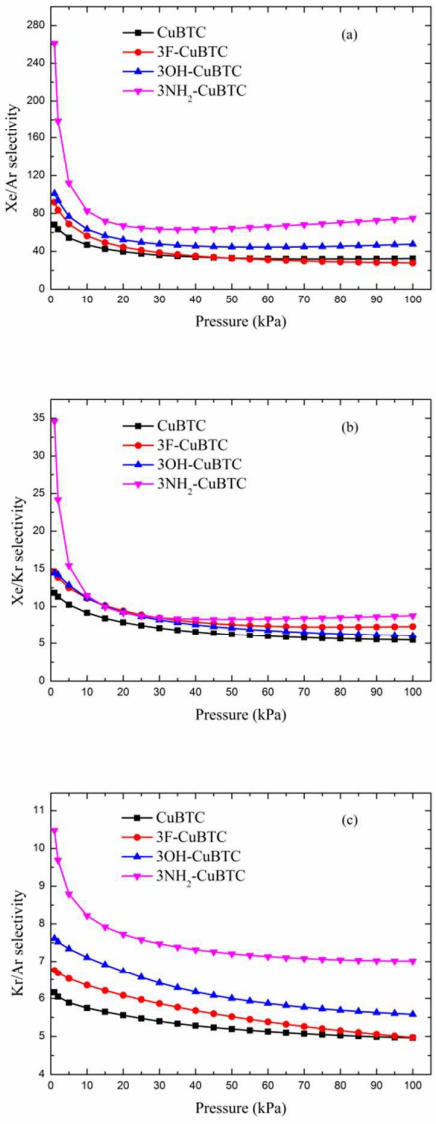

Fig. 10 Selectivities of CuBTCs for equimolar (a)Xe/Ar, (b)Xe/Kr and (c)Kr/Ar mixture.

Herein we deduce that the polarizability of the functionalized benzenes, van der Waals well depth and the electron delocalization on the aromatic ring are the main factors that dominant the

adsorption property of the functionalized CuBTC. The functionalized groups can influence the electron cloud distribution on the aromatic ring. The three inserted groups can be classified into two types: (i) the amino and hydroxyl groups are all electron-excluded groups that can averaged the positive charge from the aromatic ring and move equal number of electrons return to the aromatic ring. (ii) the fluorine atom was electron-attract group that can minify the electron density.

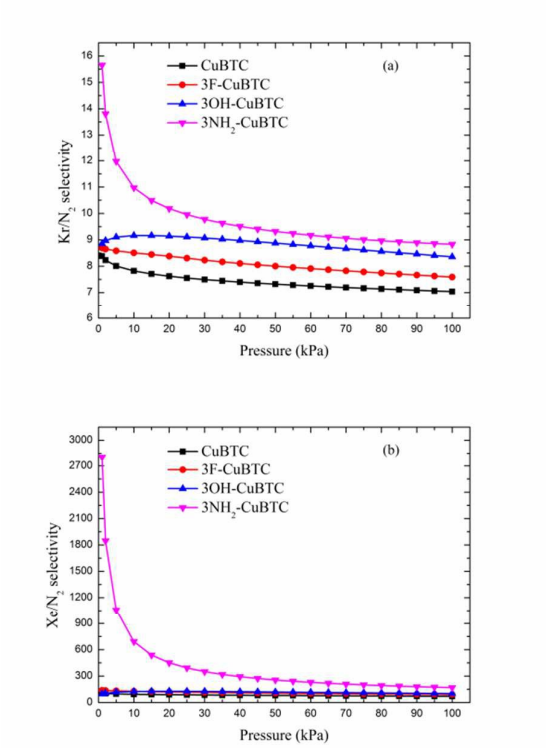

Fig. 11 Selectivities of CuBTCs for (a)Kr/N_2 and (b)Xe/N_2 mixtures including 99% molar fraction for N_2.

Conclusions

The simulation results demonstrate that mixed force field including the Universal Force Field and OPLS-AA force field are suitable to simulate the adsorption and separation of noble gases and N_2 on the CuBTC MOF. This force field was used to predict the adsorption and separation properties of noble gas and N_2 on CuBTC and functionalized CuBTC. The simulation results exhibited that amino functionalized CuBTCs could effectively enhance the adsorption volume and separation property of noble gases over N_2 and other noble gases at low pressure. The selectivity of Xe over N_2 in $3NH_2$-CuBTC is able to maintain high value while the pressure is increased to 100kPa. Aromatic ring was found to be attractive to noble gases and N_2 for its rich electron cloud that can induce these gases to stay above the ring. The gas with larger van der Waals well depth can be attractively adsorbed in CuBTCs and the functionalized groups with larger van der Waals well depth and smaller size can enhance the adsorption and separation of noble gas over N_2 and other noble gases. The high polarizability and electron cloud density of the best binding sites can also contribute to the adsorption and separation of noble gas over N_2 and other noble gases. More functionalized CuBTCs should be further investigated to explore the adsorption and separation mechanism.

Acknowledgements

We gratefully acknowledge the financial support from the National Natural Science Foundation of China (Nos.21436005 and 21576094), the National High Technology Research and Development Program of China (No.2013AA065005), SRFDP (No.20130172110012) and Guangdong Natural Science Foundation (S2011030001366).

Notes and references

1 Z. T. Lu, P. Schlosser, W. M. Smethie, N. C. Sturchio, T. P. Fischer, B. M. Kennedy, R. Purtschert, J. P. Severinghaus, D. K. Solomon, T. Tanhua and R. Yokochi, *Earth-Science Reviews,* 2014, **138**, 196-214.
2 P K. Thallapally, J. W. Grate and R. K. Motkuri, *Chem.Commun,* 2012, **48**, 347-349.
3 Z. Liu, T. Araki, Y. Okajima, M. Albert and H. Hatabu, *Eur J Radiol,* 2014, **83**, 1282-1291.
4 T. Fujino, M. Furuki, M. Kashitani, K. Onda, J. Kubota, J. N. Kondo, A. Wada, K. Domen, C. Hirose, F. Wakabayashi, M. Ishida, F. Goto and S. S. Kano, *J.Chem.Phys,* 1996, **105**, 279-288.
5 A. Ringbom, T. Larson, A. Axelsson, K. Elmgren and C. Johansson, *Nuclear Instruments and Methods in Physics Research Section A: Accelerators, Spectrometers, Detectors and Associated Equipment,* 2003, **508**, 542-543.
6 Masumeh Foroutan and Amir Taghavi Nasrabadi, *Chem.Phys. Lett.,* 2010, **497**, 213-217.
7 Masumeh Foroutan and Amir Taghavi Nasrabadi, *Physica E: Low-dimensional Systems and Nanostructures,* 2011, **43**, 851-856.
8 Najam ul Qadir, Syed A.M. Said, Haitham M. Bahaidarah, *Microporous and Mesoporous Materials,* 2015, **201**, 61-90.
9 Xuelian Su, Zizhu Yao, Yingxiang Ye, Heng Zeng, Gang Xu, Ling Wu, Xiuling Ma, Qian-Huo Chen, Lihua Wang, Zhangjing Zhang,, Shengchang Xiang, *Inorg. Chem,* 2016, **55**, 983-986.
10 Yuan Chen, Ziyin Li, Qing Liu, Yangcan Shen, Xiuzhen Wu, Dandan Xu, Xiuling Ma, Lihua Wang, Qian-Huo Chen, Zhangjing Zhang, Shengchang Xiang, *Cryst. Growth.Des,* 2015, **15**, 3847-3852.
11 R. J. Li, M. Li, X. P. Zhou, D. Li and M. O'Keeffe, *Chem.Commun,* 2014, **50**, 4047-4049.
12 J. Lee, O. K. Farha, J. Roberts, K. A. Scheidt, S. T. Nguyen and J. T. Hupp, *Chem.Soc.Rev,* 2009, **38**, 1450-1459.
13 Joonho Park, Heejin Kim and Yousung Jung, *J.Phys.Chem. Lett,* 2013, **4**, 2530-2534.
14 Bappaditya Gole, Arun Kumar Bar and Partha Sarathi Mukherjee, *Chem.Commun,* 2011, **47**, 12137-12139.
15 QingLin Li, JiaPing Wang, WeiCong Liu, XiaoYi Zhuang, JianQiang Liu, GuiLing Fan, BaoHong Li, WeiNa Lin and JianHui Man, *Inorg.Chem.Commun,* 2015, **55**, 8-10.
16 Jeffery A. Greathouse, Tiffany L. Kinnibrugh and Mark D. Allendorf, *Ind. Eng. Chem. Res.,* 2009, **48**, 3425-3431.
17 M. V. Parkes, C. L. Staiger, J. J. th Perry, M. D. Allendorf and J. A. Greathouse, *Phys.Chem.Chem.Phys,* 2013, **15**, 9093-9106.
18 Qian Wang, Hui Wang, Shuming Peng, Xuan Peng and Dapeng Cao, *J.Phys.Chem.C,* 2014, **118**, 10221-10229.

19 Stephen S.-Y. Chui, Samuel M.-F. Lo, Jonathan P. H. Charmant, A. Guy Orpen and Ian D. Williams, *Science,* 1999, **283**, 1148-1150.
20 Jinchen Liu, Jeffrey T. Culp, Sittichai Natesakhawat,Bradley C. Bockrath,Brian Zande,S.G.Sankar, Giovanni Garberoglio and J. Kar Johnson, *J. Phys. Chem. C,* 2007, **111**, 9305-9313.
21 Zhijian Liang, Marc Marshall and Alan L. Chaffee, *Energy & Fuels,* 2009, **23**, 2785-2789.
22 Lomig Hamon, Elsa Jolimaître and Gerhard D. Pirngruber, *Ind. Eng. Chem. Res.,* 2010, **49**, 7497-9503.
23 Anastasios I. Skoulidas, *J. Am.Chem. Soc.,* 2004, **126**, 1356-1357.
24 Marie V. Parkes, Hakan Demir, Stephanie L. Teich-McGoldrick, David S. Sholl, Jeffery A. Greathouse and Mark D. Allendorf, *Microporous and Mesoporous Materials,* 2014, **194**, 190-199.
25 Yeliz Gurdal and Seda Keskin, *The Journal of Physical Chemistry C,* 2013, **117**, 5229-5241.
26 Sarah Couck, Joeri F. M. Denayer, Gino V. Baron, Tom R´my, Jorge Gascon and Freek Kapteijn, *J. Am. Chem. Soc.,* 2009, **131**, 6326-6327.
27 Yang Cai, Yadong Zhang, Yougui Huang, Seth R. Marder and Krista S. Walton, *Cryst. Growth.Des.,* 2012, **12**, 3709-3713.
28 Qingyuan Yang and Chongli Zhong, *J. Phys. Chem. B,* 2007, **110**, 17776-17783.
29 Frisch M J, Trucks G W and Schlegel H B, *Wallingford, CT,* 2009, **19**, 227-238.
30 Michael Fröba Katharina Peikert and Frank Hoffmann, *Chem. Commun.,* 2012, **48**, 11196-11198.
31 Yang Cai, Ambarish R. Kulkarni, You-Gui Huang, David S. Sholl, and Krista S. Walton, *Cryst. Growth Des.,* 2014, **14**, 6122-6128.
32 C. J. Casewit A. K. Rappe, K. S. Colwell, W. A. Goddard III and W. M. Skid, *J. Am. Chem. Soc.,* 1992, **114**, 10025-10035.
33 William L. Jorgensen, David S. Maxwell and Julian Tirado-Rives, *J. Am. Chem. Soc.,* 1996, **118**, 11225-11236.
34 John J. Perry, Stephanie L. Teich-McGoldrick, Scott T. Meek, Jeffery A. Greathouse, Maciej Haranczyk and Mark D. Allendorf, *J. Phys. Chem. C.,* 2014, **118**, 11685-11698.
35 R. J. M. PELLENQ & P. E. LEVITZ, *Mol. Phys.,* 2002, **100**, 2059-2077.
36 J. J. van Loef, *Physical B & C,* 1981, **103**, 133-157.
37 Jeffrey J. Potoff and J. Ilja Siepmann, *AICHE J.,* 2001, **47**, 1676-1682.
38 Tina Düren and Randall Q. Snurr, *J. Phys. Chem.B.,* 2004, **108**, 15703-15708.
39 Materials Studio 5.0; Accelrys: San Diego, Ca, 2010.
40 Orhan Talu and Alan L. Myers, *AICHE J.,* 2001, **7**, 1160-1168.
41 Matthias Heuchel, Randall Q. Snurr and Eckhard Buss, *Langmuir,* 1997, **13**, 6795-6804.
42 S. F. Boys and F. Bernardi, *Molecular Physics,* 1970, **19**, 553-566.
43 Marc Schiltz, Roger Fourme and Thierry Prange´, *Methods In Enzymology,* 2003, **374**, 83-119.
44 Lev Sarkisov and Alex Harrison, *Molecular Simulation,* 2011, **37**, 1248-1257.
45 A. L. MYERS and J J. M. PRAUSNITZ, *A.I.Ch.E. ,* 1965, **11,** 121-127.
46 Shengchang Xiang, Yabing He , Zhangjing Zhang, Hui Wu, Wei Zhou, Rajamani Krishna and Banglin Chen, *Nat.Commun,* 2012, **3**, 1-9.
47 Youn-Sang Bae, Omar K. Farha, Joseph T. Hupp and Randall Q. Snurr, *J. Mater. Chem.,* 2009, **19**, 2131-2134.
48 Bei Liu, Qingyuan Yang, Chunyu Xue, Chongli Zhong, Biaohua Chen and Berend Smi, *J. Phys. Chem. C,* 2008, **112**, 9854-9860.

Graphical Abstract